JRC Scientific and Technical Reports

Explosions in complex geometries - a comparison of several approaches

Martin Larcher, Folco Casadei

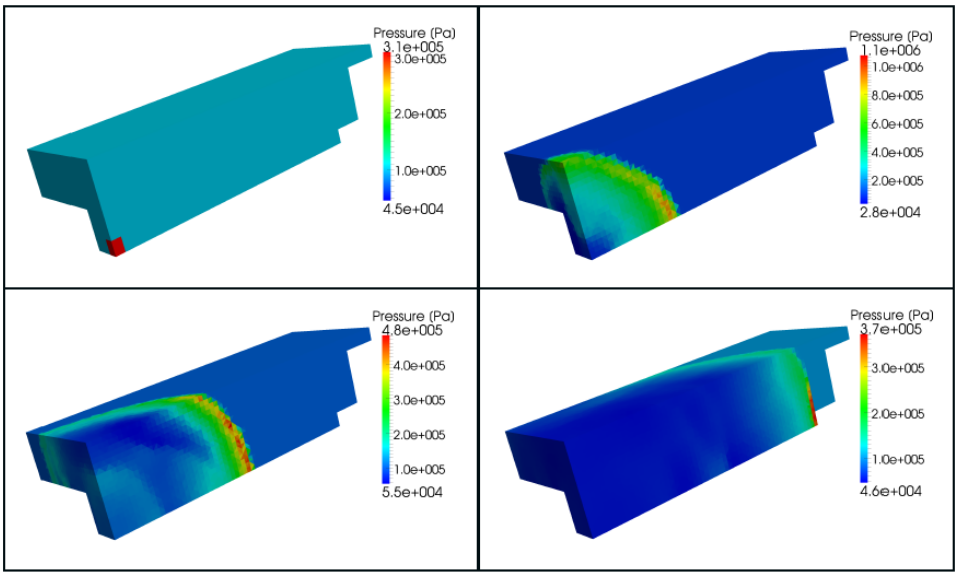

EUR 24288 EN - 2010

JRC EUROPEAN COMMISSION

ipsc Institute for the Protection and Security of the Citizen

The mission of the JRC-IPSC is to provide research results and to support EU policy-makers in their effort towards global security and towards protection of European citizens from accidents, deliberate attacks, fraud and illegal actions against EU policies.

European Commission
Joint Research Centre
Institute for the Protection and Security of the Citizen

Contact information
Address: Martin Larcher, T.P. 480, Joint Research Centre, I-21027 Ispra, ITALY
E-mail: martin.larcher@jrc.it
Tel.: +390332789004
Fax: +390332789049

http://ipsc.jrc.ec.europa.eu/
http://www.jrc.ec.europa.eu/

JRC 57322

EUR 24288 EN
ISBN 978-92-79-15245-0
ISSN 1018-5593
DOI 10.2788/73796

Luxembourg: Office for Official Publications of the European Union

Printed in Italy

Explosions in complex geometries - a comparison of several approaches

Martin Larcher, Folco Casadei

Abstract

For the design and calculation of structures loaded by air blast waves, especially from inside the structure, assumptions on the applied load are needed. This paper presents several simulation methods for the air blast loading of structures and their ability to be used for complex geometries. Experimental-analytical pressure-time functions of spherical load conditions applied to the structure by disregarding the air are not applicable in such cases because they do not account for reflections, shadowing and channelling effects. Fluid calculations, which model also the solid explosive, are very expensive due to the extremely small elements for the explosive and the air nearby.

This paper therefore presents a review of a well-known simulation method, which uses a balloon with compressed air instead of the explosive. A procedure is developed which makes it possible to determine the overpressure of such a balloon for a given size of the explosive more accurately than before. The pressure-time function and the impulse-distance function of calculations using this method show good correspondence with experimental-analytical data. The functioning of the method is verified against experimental results.

1 Introduction

Safety-sensitive buildings have to be designed against extreme dynamic loads. In addition to loads due to earthquakes and the impact of vehicles, making these structures resistant to air blast loads e.g. from terrorist attacks, becomes more and more important.

There are several risks for buildings and other engineering structures loaded by explosions. Usually it takes a relatively big charge to damage a complete structure in such a way as to cause progressive collapse. However, the load whereby people are injured by the blast wave or by flying debris is

much smaller. In the case of an explosion inside a train station, for example, the most fragile part is the glazing. The glass failure occurs depending on the type of material used (e.g. annealed or safety glass) and results in flying debris, but also in a relief surface for the air blast wave.

To design buildings and other structures against air blast waves, the loading resulting from such waves needs to be known. In most cases, the behaviour of structures under air blast load is computed by the finite element method. The loading should therefore be compatible with this method. Several methods can be found in the literature.

The behaviour in the explosive and in the surrounding air can be calculated by the well-known Jones-Wilkins-Lee (JWL) equation (see Lee et al. [1] and for the parameters of the equation Dobratz and Crawford [2]). Liu et al. [3] present a work using smooth particle hydrodynamics (SPH) to determine the pressure inside an explosive. More often used are arbitrary Lagrangian Eulerian (ALE) meshes (Cendón et al. [4], Alia and Souli [5]). Fluid calculations are very much influenced by the element size, as shown by Cendón et al. [4].

The influence of air blast waves on structures is for example investigated experimentally by Langdon and Schleyer [6] and by Gram et al. [7] with a blast simulator. Numerical investigations are presented by Langdon and Schleyer [8], Luccioni et al. [9]. The design of buildings against air blast waves is discussed by Smith and Rose [10]; the influence of a protective barrier on the blast wave is described by Zhou and Hao [11].

The present work concerns mainly the mid- and far-field where the geometry of the charge has small influence. Several blast models and tools are available to calculate the pressure at a given distance from the charge for spherical and hemispherical conditions (see Section 2.2).

The behaviour of air blast waves in complex geometries like cities is investigated by Smith and Rose [12]. Their paper shows that shielding and channelling has to be considered in urban city streets. This can be done for simple geometries using several charts. For more complex geometries numerical investigations should be used instead (see e.g. Remennikov and Rose [13]). Experimental data for explosions between buildings are given by Smith et al. [14] and Fairlie [15]. The interaction with the buildings in combination with a damage criterion is shown by Luccioni et al. [16].

This work presents several simulation methods for the air affected by explosions inside large, complex structures. The first part of the work describes the pressure behaviour of an air blast wave and compiles a set of equations from the literature, which can describe the pressure of a spherical air blast wave. Several simulation methods are then presented and compared on the basis of the calculation time and of their capability to simulate the real be-

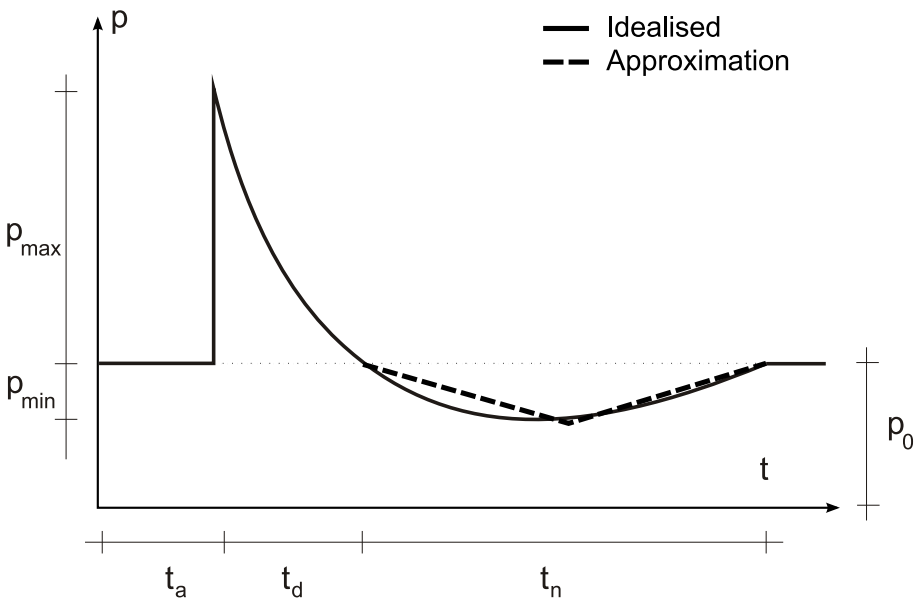

Figure 1: Pressure-time curve for a free air blast wave, approximation: dashed line

haviour inside complex structures. This is done using two experiments with different geometries.

2 Air Blast Waves

Air blast waves result from a rapid release of energy. Here, the air blast waves investigated result from the detonation of a solid explosive. Other phenomena such as the combustion of gas/air mixtures can also result in an air blast wave. Most of the models presented are also applicable to other types of detonation using an equivalent of the released energy.

2.1 Behaviour of Air Blast Waves

The pressure magnitude of a spherical air blast wave arriving at a certain point depends on the distance and on the size of the charge. An idealised form of a pressure-time function at a certain distance from the explosive is shown in Figure 1.

The main characteristics of a free field air blast wave are the following:

- The shock wave of the air blast arrives at the point under consideration

at the **arrival time** t_a. This period is defined as the time from the beginning of the explosion including the time of the detonation itself.

- The pressure attains its maximum (**peak overpressure** $p_{\max}$) very fast (extremely short rise time). The pressure then starts decreasing until it reaches the **reference pressure** p_0, which in most cases is the atmospheric pressure.

- The **duration of the positive phase** t_d is the time taken to reach this reference pressure. After this point the pressure drops below the reference pressure to the **maximum negative pressure** $p_{\min}$; then it rises again up to the atmospheric value. The **duration of the negative** phase is denoted as t_n.

- The overpressure impulse (positive impulse) is the integral of the overpressure curve over the positive phase t_d.

The idealised (free air blast) form of the pressure wave in Figure 1 can be greatly altered by the morphology of the medium encountered along its propagation. Reflections depend on the geometry, the size and the angle of incidence. The situation is much more complicated if there are several reflection boundaries, as happens between buildings.

All parameters of the pressure-time curve are usually written in terms of the scaled distance:

$$Z = \frac{d}{\sqrt[3]{M}} \tag{1}$$

where M is the mass of the explosive charge in kg of equivalent TNT and d the distance from the centre of the charge in m.

2.2 Experimental, Analytical and Numerical Data

A widely used way of describing the form of an air blast wave is the so-called modified Friedlander equation (see e.g. Baker [17]), which proposes a function for the positive phase of the air blast wave. The pressure p at time t can be calculated with:

$$p(t) = p_0 + p_{\max}\left(1 - \frac{t}{t_d}\right)^{-\frac{bt}{t_d}} \tag{2}$$

The slope of the pressure-time function can be adapted with the form parameter b, which can be taken from Baker et al. [18]. All parameters of Equation (2) can be taken from several diagrams and equations (e.g. Baker [17], Kinney and Graham [19], Kingery and Bulmash [20]). Also widely used is the

software CONWEP [21], which provides the results of US Army Manual TM 5-855-1 [22].

Kingery and Bulmash [20] present equations for the peak overpressure, the duration of the positive phase, the positive impulse, and the arrival time. All these values are available for incident and reflected waves for spherical (free field) as well as for hemispherical conditions. In this paper these functions are used. For the negative peak pressure a diagram proposed by Drake et al. [23] is used.

The above pressure-time curve can be used for a simulation method which uses a load-time function (see Section 3.3). In addition, this equation can be compared with numerical results. The expression of the impulse for the positive part is also used to fit the balloon method (see Section 3.5).

3 Numerical Investigations

All numerical calculations presented are performed with EUROPLEXUS (see [24]), an explicit finite element code for non-linear dynamic analysis developed in collaboration between the French Atomic Energy Commission (CEA) and the Joint Research Centre (JRC) of the European Commission. The main focus of EUROPLEXUS is on fluid-structure interaction in fast dynamics.

3.1 Material Laws

The present investigations do not use full-fledged fluid-structure interaction (except the last example in Section 4.3). The reflected pressure is in fact calculated by neglecting the deformability of the structure, i.e. by assuming infinitely rigid structural boundaries. Two materials are used for the calculations: the ideal gas equation for the air and the JWL equation for the explosive.

3.1.1 Ideal Gas Equation for Air

The pressure p of the air follows the ideal gas equation:

$$p = \rho(\gamma - 1)e_{\text{int}} \tag{3}$$

The heat capacity ratio γ (assumed here as constant) is set to 1.35, whereas the density of the air at normal atmospheric pressure ($p_0 = 10^5\,\text{Pa}$) is $\rho_0 = 1.3\,\text{kg/m}^3$, which leads to a specific internal energy at atmospheric pressure of $e_{\text{int},0} = 2.1978 \cdot 10^5\,\text{J/kg}$.

Absorbing material is used to impose non-reflecting boundary conditions along open fluid boundaries, which allows to cut the air model at locations where reflections do not have to be considered. The model consists simply in applying a fictitious external pressure $p = -\rho c v_n$, where ρ is the density of the material at the boundary, c its sound speed and v_n the normal component of the particle velocity at the boundary.

3.1.2 JWL Equation for Explosive

The explosive is modelled with the Jones-Wilkins-Lee (JWL) equation of state, which provides a good approximation of the pressure release from an explosive material. The pressure p can be calculated with the following formula:

$$p = A(1 - \frac{\omega}{R_1\bar{\rho}})\, e^{-R_1\bar{\rho}} + B(1 - \frac{\omega}{R_2\bar{\rho}})\, e^{-R_2\bar{\rho}} + \omega\, \rho\, e_{\text{int}} \tag{4}$$

where $\omega = \gamma - 1$. A, B, R_1, and R_2 are constants depending on the kind of explosive and are given in Table 1. e_{int} is the specific internal energy at atmospheric pressure. The quantity $\bar{\rho}$ is the relative density, defined as:

$$\bar{\rho} = \frac{\rho_{\text{sol}}}{\rho} = \frac{V}{V_{\text{sol}}} \tag{5}$$

where ρ_{sol} is the density of the explosive in solid state, ρ is the current density and V is the volume. The first and second terms in (4) describe the behaviour during the detonation, whereas the behaviour of the air after the energy release is represented by the last term, which corresponds to the perfect gas law (3).

The parameters for the JWL equation can be found, for example, in Dobratz and Crawford [2]. The values used for TNT and C4 explosives are shown in Table 1. The release of pressure is combined with an ignition law, which uses the detonation velocity v_{det}.

3.2 Finite Elements (FE) – Finite Volumes (FV)

In this work calculations are performed using the finite element method as well as using the finite volume method. All calculations use Eulerian meshes since the deformation of structures is not considered (except in Section 4.3, where ALE is used). An explicit time integration scheme is used.

The finite volumes (for the implementation used, see Galon [25]) use a second-order approach for the flux in order to improve the calculation of

	Unit	TNT	C4
A	Pa	$3.738 \cdot 10^{11}$	$5.98155 \cdot 10^{11}$
B	Pa	$3.747 \cdot 10^{9}$	$0.13750 \cdot 10^{11}$
$e_{\text{int},0}$	J/kg	$3.68 \cdot 10^{6}$	$5.4341 \cdot 10^{6}$
R_1	-	4.15	4.5
R_2	-	0.90	1.5
ω	-	0.35	0.32
ρ_{sol}	kg/m^3	1630	1601
v_{det}	m/s	6930	8500

Table 1: JWL parameters for some explosive materials (from [2])

shock discontinuity with respect to the first-order approach typically used in finite elements.

The oscillations occurring after a shock wave are a disadvantage of second-order approaches. There are several possibilities to reduce these oscillations after a shock front. Often used in fast-dynamic numerical simulations is the classical artificial viscosity (see e.g. Benson [26]). A pseudo-viscous pressure term is built from the velocity, the density and the sound speed and is then added to fluid pressure.

Another possibility to reduce the oscillations is to use special flux limiters developed for finite volumes. The limitation is achieved by using special rules for the combination of the first- and of the second-order approaches. Several examples are given in Galon [25]. The limiter proposed by Dubois [27] is used for the present calculations. Flux Corrected Transport (FCT, see Boris and Book [28]), which is used by AUTODYN [29], is a similar limitation.

3.3 Simulation Methods

There are several methods of numerical modelling that can be used in order to load a structure with an air blast wave. These methods differ in the number of finite elements (or finite volumes) used and, accordingly, in the calculation time.

- The **solid TNT model** describes the mechanical behaviour of the (initially solid) explosive with a material law, e.g. the JWL equation (4). A fine mesh is essential to obtain realistic results. The size of the elements in the region around the explosive should be much smaller than the size of the explosive charge. These calculations are therefore very expensive. To reduce the computation time, spatial partitioning (see

Casadei and Halleux [30]) can be used, which reduces the calculation time for models with a large spectrum of element sizes.

- The computational explosion and blast assessment model proposed by Clutter and Stahl [31] is also a solid TNT model that uses only one element for the explosive. This is possible using several special methods in combination with the Becker-Kistiakowsky-Wilson EOS for the explosive.

- 1D to 3D **mapping**. This method is used, for example, in AUTODYN (see remapping manual [32] and Birnbaum et al. [33]), and is also a solid TNT model. A 1D calculation is used until the air blast wave reaches a surface. Then the values of the density, energy, velocity, and pressure are mapped onto a 3D mesh. Rose and Smith [34] map the 1D model to 2D when the wave arrives at the first surface and map the 2D model to 3D when the wave arrives at a second surface with another direction. This method is a combination of the solid TNT and of the control volume methods. The calculation time should therefore be shorter than for the solid TNT model. This method is provided only by some numerical codes.

- **Compressed balloon method** (phenomenological model). The pressure-time function resulting from a compressed balloon can approximately match the curve of an air blast wave. The amount of compression can be calibrated with the maximum pressure or the impulse. The calculation time is smaller than for the solid TNT model. This method is described in detail later on.

- **Control volume**. A volume around the explosive is loaded by a pressure-time curve. This curve can be taken, for example, from Kingery and Bulmash [20]. An initial velocity has to be applied to the air particles. The air inside the control volume can be removed. This leads to a reflection at the surfaces of the control volume, which can be neglected if the control volume is small. In contrast, the air inside the control volume can also be modelled. Then, the applied pressure wave is also produced inside the control volume, which results in a reflection inside the control volume. This method should be therefore validated through comparisons with calculations using the solid TNT model. The computation time is similar to that of the compressed balloon approach. The method is suitable for Eulerian calculations far away from the explosive (planar blast loads), where the control volume transforms into

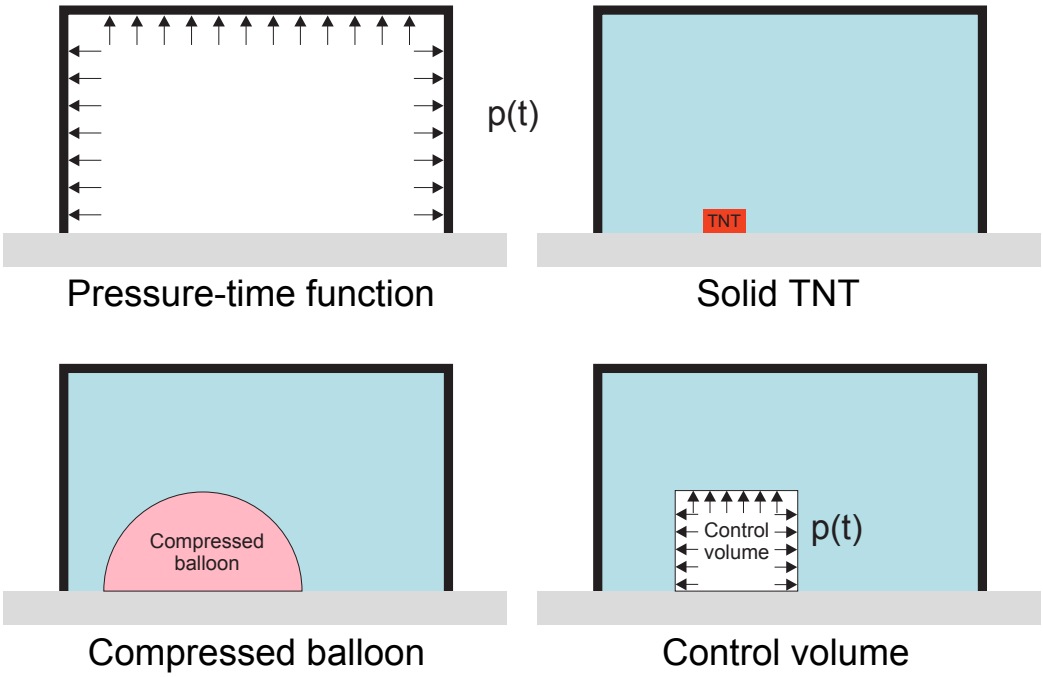

Figure 2: Simulation methods

a surface of the air which is subjected to a pressure-time function. This procedure is used, for example, by Børvik et al. [35].

- **Load-time function** (phenomenological model). This is only usable for an estimation of the behaviour of a structure loaded by an air blast wave. The structure is loaded by a load-time function built with the pressure-time function presented in Chapter 2. The calculation is relatively inexpensive. Alternatively, the pressure-time function can be determined by means of a fluid pre-calculation with fixed boundaries for the structure. The structure is then loaded by the pressures resulting from this fluid calculation.

The choice among these methods depends on the scope of the analysis. Figure 2 sketches four of the above described methods for the simulation of an air blast wave. The differences between the methods are summarised in Table 2.

Method	air/structure	reflections, channelling	calculation time
Solid TNT	air and structure	considered	very long
Mapping	air and structure	considered	medium
Compressed balloon	air and structure	considered	medium
Control volume	air and structure	(considered)	medium
Load-time function	only structure	not considered	short

Table 2: Comparison of various simulation methods

3.4 Solid TNT Model

First, the solid TNT model is tested for its capacity to simulate air blast waves. A rectangular parallelepiped model with dimensions 2.2 x 0.6 x 0.6 m is used to compare the experimental results of Kingery with numerical results. The element size of the tetrahedral elements is chosen as 0.005, 0.0067, and 0.01 m respectively. Three symmetry surfaces are used to calculate only one eighth of the model (i.e. 1.1 x 0.3 x 0.3 m). The other three surfaces of the parallelepiped are defined as absorbing boundaries. The corresponding mass of the explosive (TNT) in the 1/8 model is 1.6 kg. One eighth of the charge is modelled as a sphere by setting the elements inside a sphere of 0.062 cm radius as explosive ('spherical' charge). The pressure is recorded at the following measuring points: P1(0.5/0.1/0.1), distance 0.52 m from the charge centre and P2(0.9/0.1/0.1), distance 0.91 m.

Figures 3 and 4 show that the solution using finite elements results in smaller pressures and in an additional time lag compared with the experimental results. The time lag and the difference between the numerical and experimental pressures increase with the distance. The finite element model can represent the impulse for the intermediate and for the fine mesh investigated (see Table 3). For finite element calculations, this effect increases with the distance from the charge. The influence of the element sizes is observable but small. Also a cubical charge instead of the spherical one has, apart from a time lag, only a small influence on the pressure time curve.

The cubic charge overestimates the impulse for longer distances due to a non-perfectly spherical air blast wave.

To summarize, the finite element as well as the finite volume solution can be limited used far away from the explosive. The finite volume solution shows a better description of the wave and also over a longer distance.

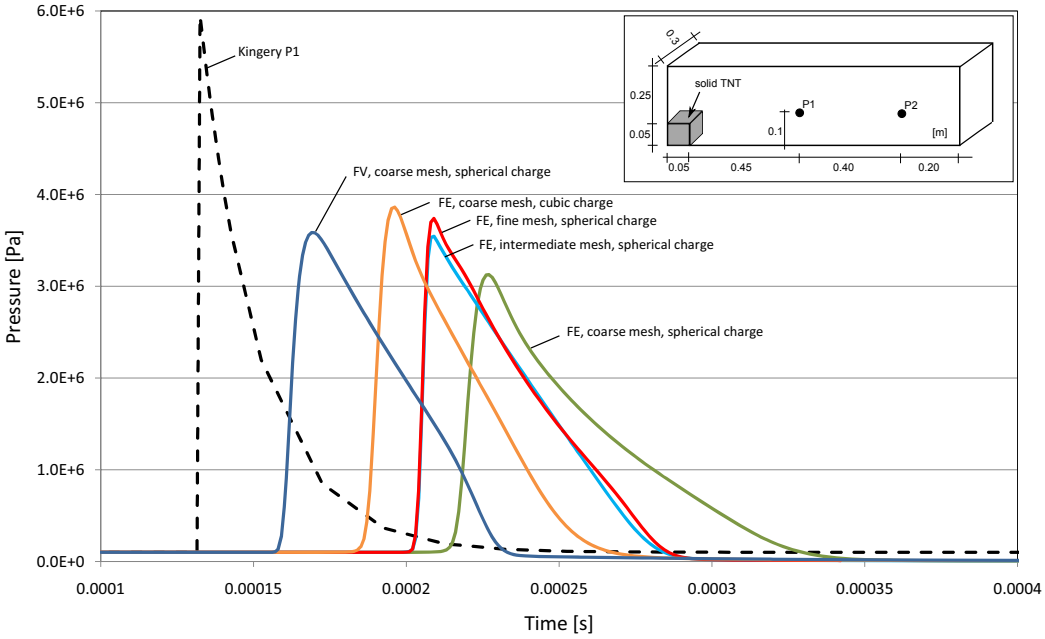

Figure 3: Solid TNT model, finite element and finite volume approach, results at measuring point P1 (distance 0.52 m)

The calculation time for solid TNT models is long. The calculation time is compared with other simulation methods in Section 4.2.

3.5 Compressed Balloon Method

The computational effort required by solid TNT models is very large. In addition, the results of this model depend very often on the size of the elements. The models which use a pressure-time function, in contrast, are sometimes not realistic due to the fact that these models do not consider reflections, street channelling and shadowing.

The idea of the balloon method is to use a region (balloon) with compressed air of initial size much bigger than the size of the solid explosive. This method goes back to Brode [36]. He proposes to use a balloon filled by gas at an initial pressure of:

$$p_{\text{Brode}} = \frac{E_{\text{TNT}}(\gamma - 1)}{V_{\text{bal}}} + p_0 \tag{6}$$

where E_{TNT} is the total initial energy of the charge, V_{bal} the volume of the balloon, p_0 the atmospheric air pressure, and γ the heat capacity ratio of the

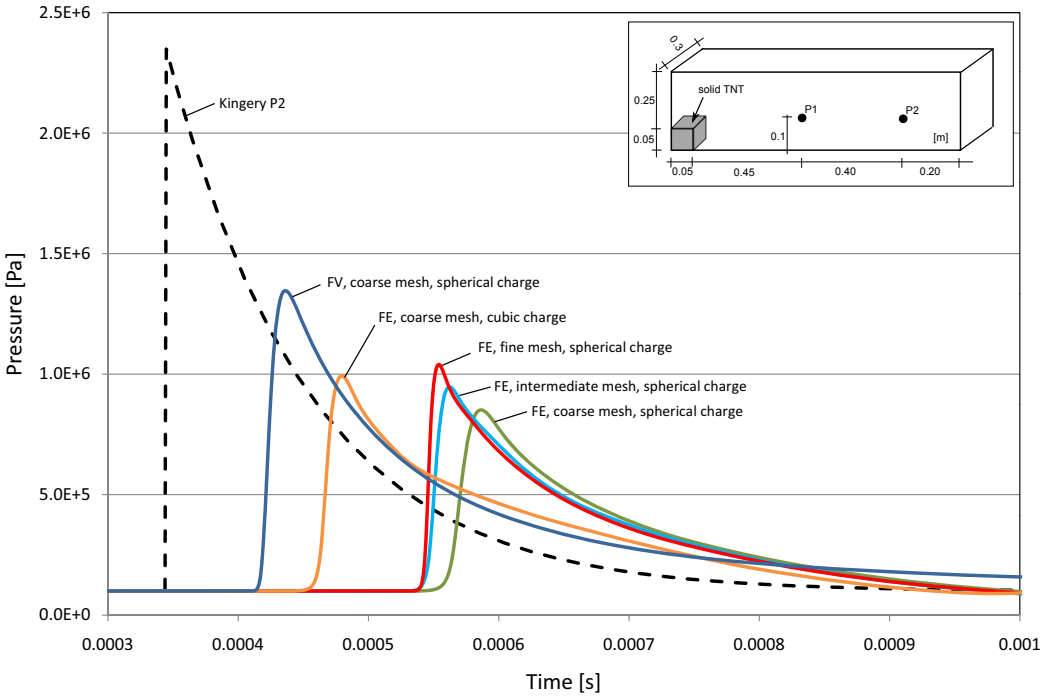

Figure 4: Solid TNT model, finite element and finite volume approach, results at measuring point P2 (distance 0.91 m)

gas in the balloon. In the literature (see e.g. Baker et al. [18]) it is customary to relate the energy of the charge (E_{TNT}, expressed in J) to the mass of the charge M_{TNT} expressed in equivalent TNT kilograms, by assuming that 1 kg of TNT releases $4.52 \cdot 10^6$ J of energy, so that:

$$E_{\mathrm{TNT}} = M_{\mathrm{TNT}} \cdot 4.52 \cdot 10^6 \tag{7}$$

Brode's equation (6) is used by several authors, e.g. Ritzel and Matthews [37] or Omang et al. [38], to calculate the far-field behaviour of an air blast wave in an easy and effective way.

Trelat [39] presents a similar experimental method that can be used to reproduce an air blast wave using balloons filled with burnable gas. The difference in the air blast characteristics (peak pressure and impulse) between the air blast wave resulting from the ignition of the gas and from solid explosive detonation can be fitted with a special equation (see [39]).

Model	$p_{max,1}$	$p_{max,2}$	i_1	i_2
Kingery	5.94E6	2.35E6	132.8	102.4
FE, coarse mesh, spherical charge	3.13E6	8.52E5	116.4	98.6
FE, intermediate mesh, spherical charge	3.54E6	9.47E5	131.8	106.9
FE, fine mesh, spherical charge	3.74E6	1.04E6	137.0	108.3
FE, coarse mesh, cubic charge	3.86E6	9.93E5	120.2	128.9
FV, coarse mesh, spherical charge	3.59E6	1.35E6	137.5	-

Table 3: Comparison of maximum pressures and impulses for different meshes

3.5.1 Development of the Balloon Method

Several calculations using a compressed balloon are done in this work to test how accurately the release of pressure from the balloon can represent the air blast waves resulting from a real explosion. For our first investigation, 3D spherical balloons are used (see Figure 5). The balloon is the red zone shown in the Figure. The surrounding air, shown in blue on the Figure, is meshed by projecting the balloon surface radially and absorbing boundary conditions are imposed along the external envelope of the model. Thanks to symmetry conditions only one eighth of the model is meshed. The model uses 40 elements in the circumferential direction (for one eighth of the sphere), and a total of 104,000 brick elements. Three different geometries are used with different sizes of the balloon radius ($R_b = 0.5, 1.0, 5.0\,\mathrm{m}$) and of the corresponding air radius ($R_{\mathrm{air}} = 5, 10, 50\,\mathrm{m}$, respectively).

The computed results (in particular the maximum pressure and the impulse) are then compared with the experimental values resulting from a real explosion. The impulse is the most important parameter as concerns air blast wave effects on a structure. A comparison of the computed impulse vs. the experimental values of Kingery and Bulmash [20] is presented in Figure 6, as a function of the scaled distance defined by Equation (1). For the simulation shown in this Figure a value of $R_b = 0.5$ m and $R_{\mathrm{air}} = 5$ m is used. The assumed mass of the charge is $M_{\mathrm{bal}} = 3.28$ kg TNT equivalent, and from Equation (6) this gives an initial balloon pressure of $10^7\,\mathrm{Pa}$.

The comparison between the impulse using Kingery's equations and the balloon model (Figure 6) shows that the latter is too small, but has the same shape over a broad range of scaled distances, except in a small region immediately adjacent to the balloon. This trend is observed in all calculations done with the geometry parameters given. Furthermore, there is no dependency on the element size. The comparison of pressures shows that the peak pres-

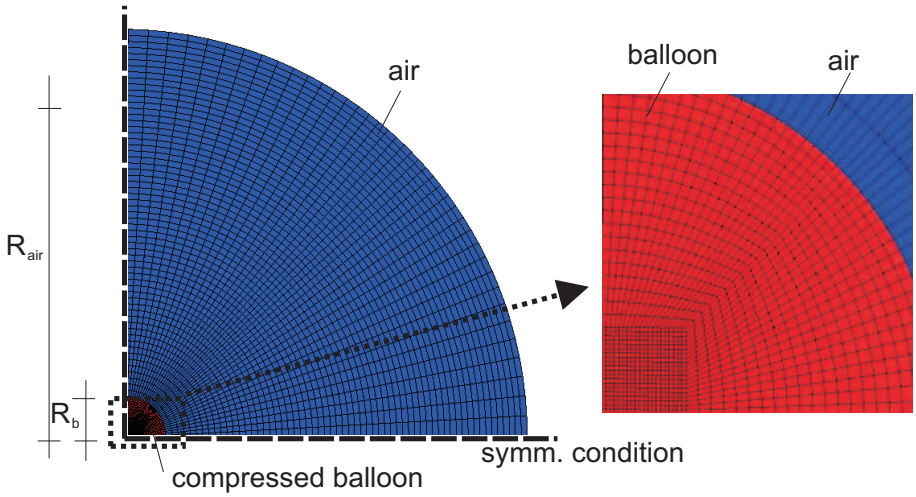

Figure 5: Compressed balloon model

sure of the compressed balloon method is similar to Kingery's experimental data (see Figure 7), again if one neglects the region immediately adjacent to the balloon.

The idea is now to introduce a correction factor α_{bal}, depending upon the mass of the charge, in order to obtain the right impulse. The easiest way to obtain this correction is to scale down the experimental curve from Kingery (which has an analytical expression) so that it best fits the balloon impulse computed numerically. In the chosen example, this occurs for a charge of approximately $M_{\text{fit}} = 2.5$ kg TNT (instead of $M_{\text{bal}} = 3.28$ kg), as shown by the dashed line in Figure 6.

In order to generalize this result, several calculations are performed, all using a compressed balloon of 0.5 m radius, but with different values of the initial pressure. To each of the computed impulse vs. scaled-distance curves, a corresponding experimental curve from Kingery is best fitted. The resulting values of TNT equivalent charges M_{fit} are represented by the lower curve in Figure 8, as a function of the over-pressure.

Note that, to allow later on the determination of the correction factor α_{bal}, the charge masses in Figure 8 are *not* plotted vs. the initial balloon over-pressure $p_{\text{Brode}}(M_{\text{bal}}) - p_0$, but rather vs. a "best fitted" initial over-pressure p_{fit}, obtained from Brode's equation (6) as follows:

$$p_{\text{fit}} = p_{\text{Brode}}(M_{\text{fit}}) - p_0 = \frac{E_{\text{fit}}(\gamma - 1)}{V_{\text{bal}}} \tag{8}$$

where $E_{\text{fit}} = M_{\text{fit}} \cdot 4.52 \cdot 10^6$ according to Equation (7). For the above example

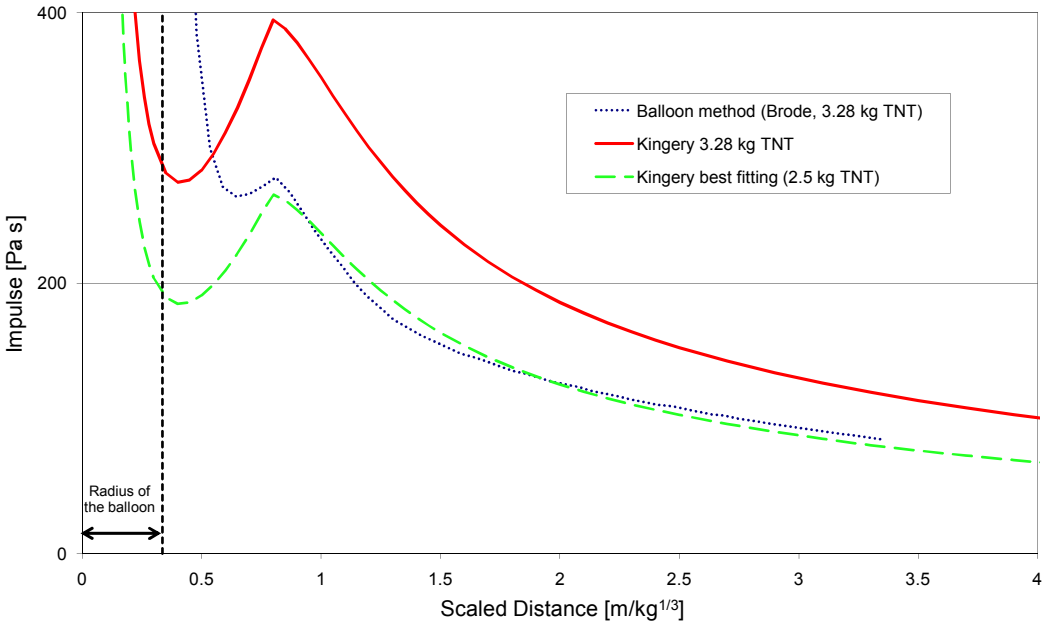

Figure 6: Comparison of the impulse of the balloon method against the experimental values of Kingery and Bulmash [20] for $R_b = 0.5\,\mathrm{m}$, $R_{\mathrm{air}} = 5.0\,\mathrm{m}$, initial balloon pressure $10^7\,\mathrm{Pa}$

the best fitting charge is $M_{\mathrm{fit}} = 2.5$ kg TNT, and this results into $p_{\mathrm{fit}} = 7.55 \cdot 10^6\,\mathrm{Pa}$.

The equivalent TNT charge of the balloon M_{bal} is represented by the upper curve in Figure 8. The two energy curves in this Figure show similar behaviour in the logarithmic scale used for the over-pressure so that, by computing the ratio between them, we obtain the scaling factor α_{bal} as a function of p_{fit} for this particular geometry ($R_b = 0.5$ m and $R_{\mathrm{air}} = 5.0$ m), see the red curve in Figure 9. The same procedure is then repeated for the other values of the balloon radius, namely $R_b = 1.0$ m and $R_b = 5.0$ m, showing very little dependency of results upon the balloon radius, see the blue and yellow curves in Figure 9, respectively.

All these curves are very close to one another and approximately linear, except perhaps for very low values of the initial balloon pressure, see comment below. They can be fitted quite accurately by the following linear expression, also plotted in Figure 9:

$$\alpha_{\mathrm{bal}} = -0.2205 \log(p_{\mathrm{fit}}) + 2.265 \tag{9}$$

where p_{fit} indicates the best-fit over-pressure in the balloon and must be

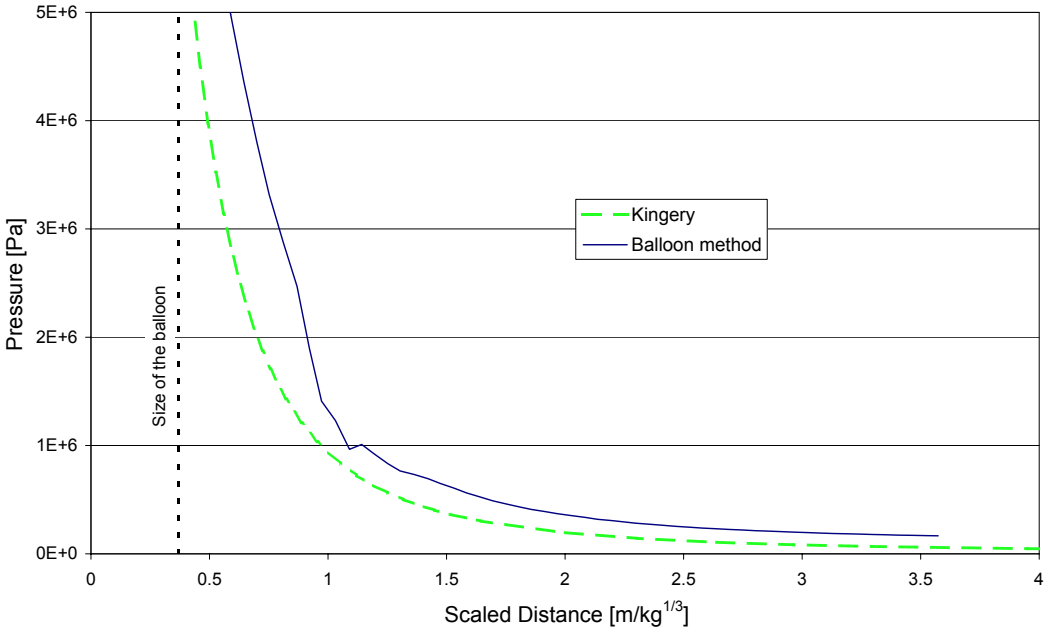

Figure 7: Comparison of the peak pressure of the balloon method against the experimental values of Kingery and Bulmash [20] for $R_b = 0.5\,\mathrm{m}$, $R_{\mathrm{air}} = 5.0\,\mathrm{m}$, initial balloon pressure $10^7\,\mathrm{Pa}$

expressed in Pa (see Equation (8)).

3.5.2 Algorithm to compute the initial balloon conditions

To summarize, the following procedure can then be used to obtain the initial pressure of the balloon p_{bal} for a given TNT equivalent mass M (in kg) and a given balloon volume V_{bal} (in m^3):

1. Calculation of the nominal energy of the explosive charge (E_{TNT}, in J) with Equation (7):
$$E_{\mathrm{TNT}} = M \cdot 4.52 \cdot 10^6 \tag{10}$$
2. Calculation of the over-pressure in the balloon in Pa with Brode's formula Equation (6):
$$p_{\mathrm{TNT}} = p_{\mathrm{Brode}} - p_0 = \frac{E_{\mathrm{TNT}}}{V_{\mathrm{bal}}}(\gamma - 1) \tag{11}$$
3. Calculation of the dimensionless scaling factor α_{bal} with Equation (9):
$$\alpha_{\mathrm{bal}} = -0.2205 \log(p_{\mathrm{TNT}}) + 2.265 \tag{12}$$

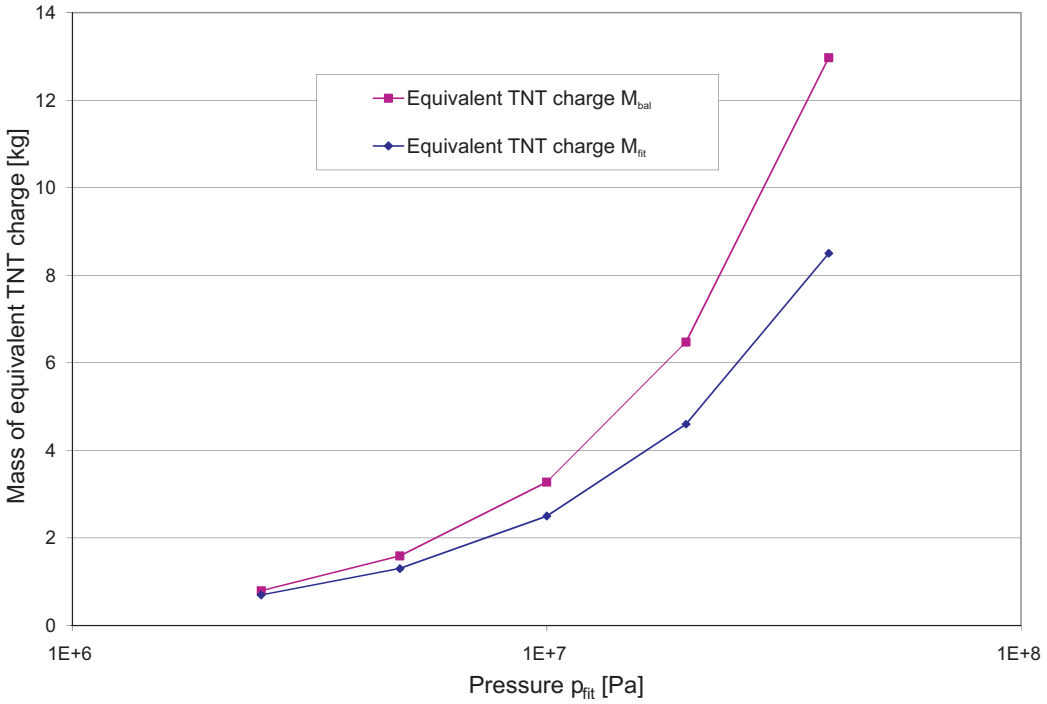

Figure 8: Charge mass vs. p_{fit} for $R_b = 0.5\,\text{m}$, $R_{\text{air}} = 5.0\,\text{m}$

4. The initial pressure in the balloon can be calculated with:

$$p_{\text{bal}} = \frac{p_{\text{TNT}}}{\alpha_{\text{bal}}} + p_0 \tag{13}$$

5. A square root factor f_{bal} is calculated in order to distribute the scaling α_{bal} "in equal parts" to the internal energy and to the density of the balloon gas (see discussion below):

$$f_{\text{bal}} = \sqrt{\frac{p_{\text{bal}}}{p_0}} \tag{14}$$

6. Finally, the values of the internal specific energy $e_{\text{int,bal}}$ and of the density ρ_{bal} of the balloon can be calculated by multiplying the values for the uncompressed air ρ_0 and $e_{\text{int},0}$ by the factor f_{bal}:

$$\begin{aligned} \rho_{\text{bal}} &= \rho_0 \cdot f_{\text{bal}} \\ e_{\text{int,bal}} &= e_{\text{int},0} \cdot f_{\text{bal}} \end{aligned} \tag{15}$$

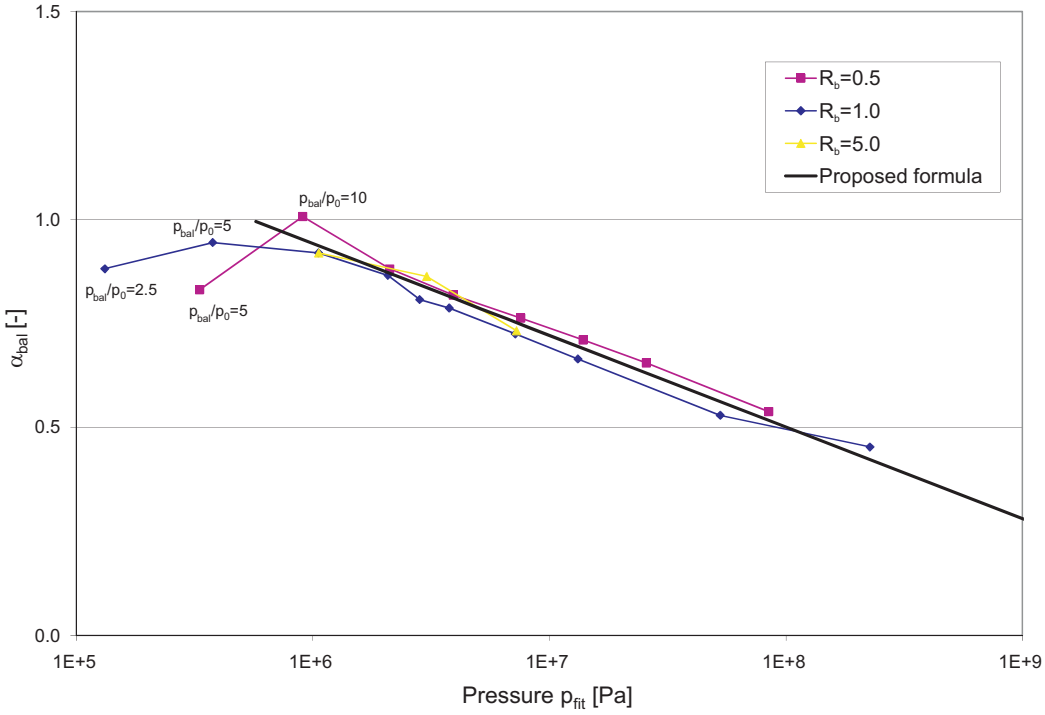

Figure 9: Scaling factor α_{bal} for different sizes of the balloon and proposed linear formula

The use of the factor f_{bal} deserves some explanation. The initial pressure of the balloon results typically from the perfect gas Equation (3) and is the combination of the higher internal energy (temperature) and the higher density of the balloon gas, with respect to atmospheric values. Therefore, for a given pressure of the balloon, only one of these two quantities is independent while the other one results from the equation of state. So in principle one can arbitrarily decide how to "distribute" the scaling factor α_{bal} between ρ and e_{int}. Numerical tests have shown that in practice there is no influence of the chosen distribution rule on results, in particular as concerns the computed impulses. Therefore, it is proposed to adopt the square root factor as given above in Equations (14) and (15).

With this simple procedure it is possible to calculate the initial state of the balloon gas for a given balloon size and a given charge. While the proposed procedure is applicable in general in any computer code, it should be noted that the coefficients appearing in Equation (12) have been calibrated for the specific Finite Volume model used in our code. If a different numerical model (e.g. Finite Elements) or a different computer code is used, the calibration

should of course be checked. For example, when using the Finite Element model for fluids also available in our code, slightly different values of the coefficients in the expression of α_{bal} (12) have to be used to obtain the best possible results with the proposed simple balloon model.

3.5.3 Limitations of the Compressed Balloon Method

The proposed procedure raises the question, whether there are limitations on the size of the balloon or on the ratio of the initial balloon pressure versus the atmospheric pressure (pressure ratio p_{bal}/p_0).

The curve of α_{bal} (see Figure 9) has some limits. Clearly, values smaller than 0.0 cannot be used, because they would result in negative pressure. But, even using values of α_{bal} less than 0.5 represents an extrapolation of the numerical data shown in Figure 9. These values should therefore be used with care (a warning is issued by the code). In addition, if the value of α_{bal} is relatively small, a small change of α_{bal} results in a large change of the overpressure. Also in that case accuracy is relatively low.

Values of α_{bal} larger than 1.0 are also dangerous, because none of the computed points in Figure 9 is above 1.0, at least for our own numerical model. Therefore, also in this case a warning is issued in our implementation.

It is observable in Figure 6 that the distance to any structure should be at least twice the radius of the balloon.

3.5.4 Influence of the Balloon Size (or Pressure Ratio)

Several calculations are performed to determine the influence of the balloon size (or pressure ratio) on the pressure-time curve. The geometry shown in Figure 10 is used. The charge has a mass of 16 g; the size of the balloon varies between 0.04 m and 0.2 m. The size of the cube-shaped finite volumes is chosen as 2 cm. Spherical conditions are used. The pressure-time curves are compared at two locations. The first point has a distance of 0.4 m (scaled distance of $1.59\,\text{m/kg}^{1/3}$) and the second point a distance of 0.8 m (scaled distance of $3.17\,\text{m/kg}^{1/3}$) from the centre of the explosive.

The calculations with small initial balloon pressures ($p_{\text{bal}}/p_0 = 5.2$) show that these models cannot reach a good agreement with the Friedlander equation (2) using Kingery's parameters (see Figure 11). The values of α_{bal} in such cases are almost 1.0 or higher. Therefore, it is recommended that only balloons with pressure ratios p_{bal}/p_0 higher than about 50 are used. If this condition is not met, the initial size of the balloon should be adjusted.

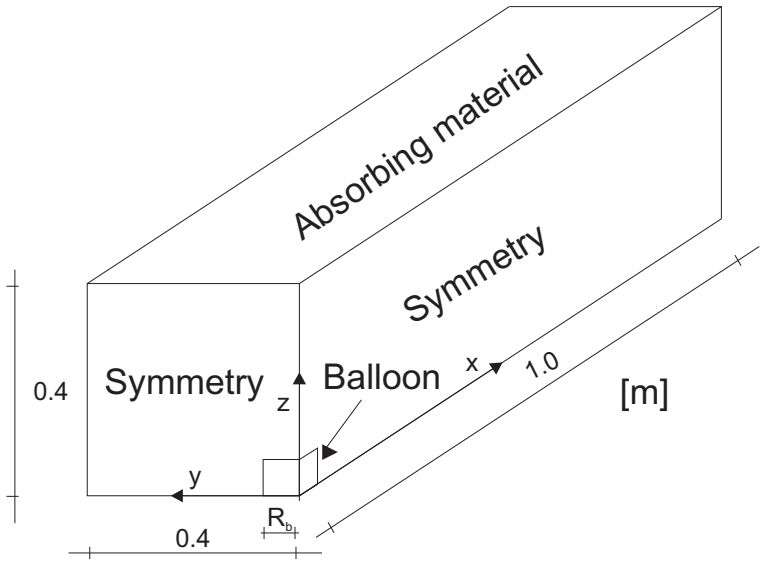

Figure 10: Model to check the influence of the balloon size (resp. overpressure) on the form of the pressure-time function

3.5.5 Influence of the Mesh Size (Convergence Study)

A convergence study is carried out to determine the influence of the size of the finite volumes. The model presented in Figure 5 is changed in such a way that the finite volumes are built by respecting an optimal aspect ratio, as shown in the inset of Figure 12. The size of the finite volumes can then be easily varied by changing the number of elements in the circumferential direction (or "segments", see Figure 12).

The computed impulses for different numbers of segments are shown in Figure 12, as a function of distance from the charge scaled to a charge of 2.5 kg TNT, to allow direct comparison of the various results. The radius of all balloons is set to $R_b = 0.5\,\mathrm{m}$; the radius of the complete model is set to $R_{\mathrm{air}} = 5.0\,\mathrm{m}$. The overpressure inside the balloon is set to $10^7\,\mathrm{Pa}$ ($p_{\mathrm{bal}}/p_0 = 100$).

The impulse-distance curves of models with more than 6 segments show very similar behaviour. All these curves result in a similar mass of the explosive charge by fitting them with the results from Kingery. Only the curve with 4 segments is not usable.

Because of this good correspondence of the results for several mesh sizes, the influence of the mesh on the impulse is quite small. While the impulse is represented well even by relatively coarse meshes, the peak pressure depends

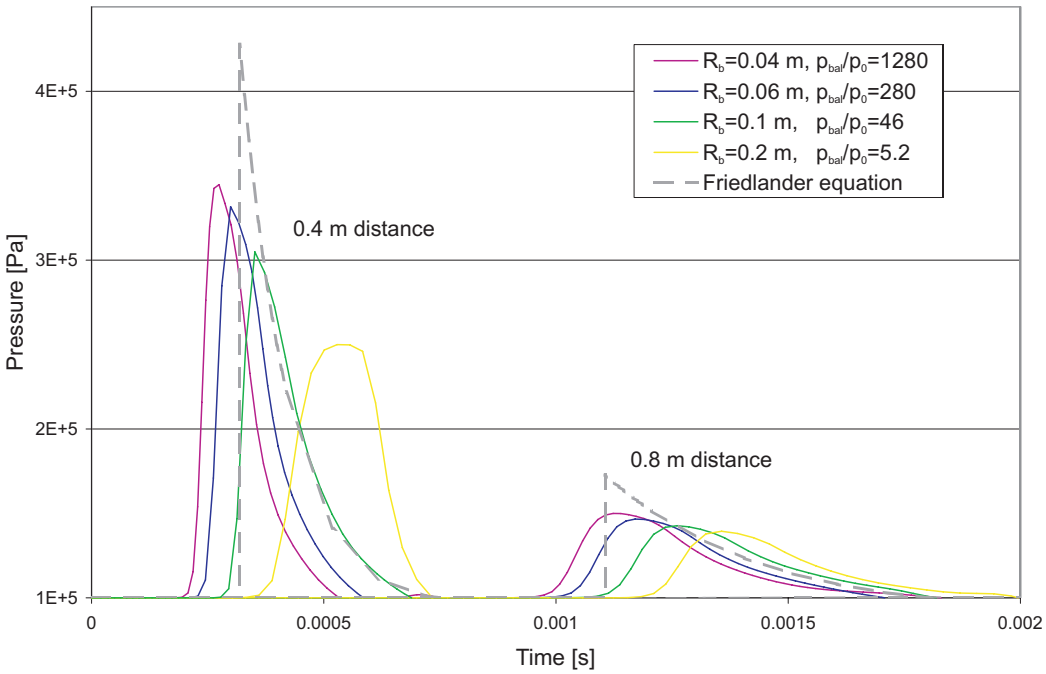

Figure 11: Influence of the balloon size (resp. overpressure) on the form of the pressure-time function. Distance to the charge: 40 cm resp. 80 cm

much more on the mesh size. The model of Section 3.5.4, see Figure 10 is used with a size of the balloon of 10 cm and different finite volume sizes using a regular mesh. The resulting pressure-time functions are shown in Figure 13. For this geometry an element size smaller than 2 cm is recommended, which corresponds to at least 5 elements in the balloon region along each spatial direction, which has also be shown in the first experiment.

4 Comparison with Experiments and Application Examples

The compressed balloon method is used to simulate several air blasts with different geometries. The results are compared with solid TNT models and with Kingery's experimental curves.

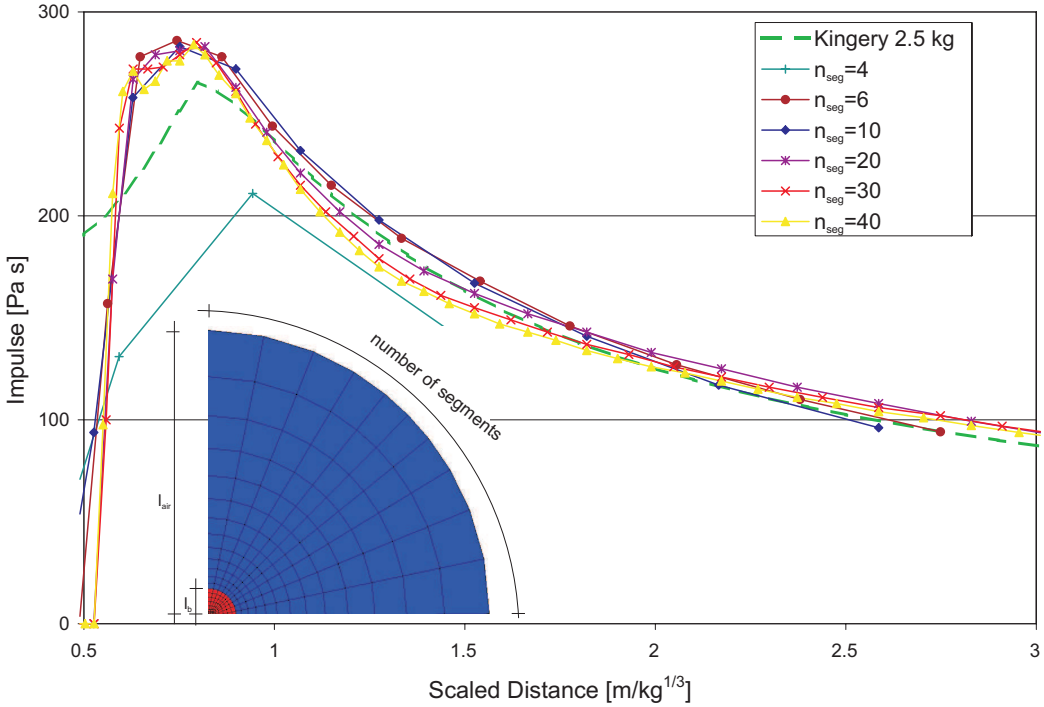

Figure 12: Influence of mesh size, $R_b = 0.1$ m – impulse

4.1 Explosion Experiment

The experiment presented by Alia and Souli [5] involves an explosion of 227 g C4 under spherical conditions, corresponding to 268 g TNT (see Cusatis et al. [40]). The explosive is placed at a distance of 1.22 m from a rigid wall. The pressure wave is reflected by this wall. The pressure is measured above the explosive at a distance of 1.52 m from the charge. The geometry of the numerical models is presented in Figure 14.

Five different numerical simulations of this experiment are performed: two with the solid TNT model and the others with the balloon method.

Due to the fact that the wave reflected by the wall hits the pressure gauge after a relatively long time, the wall is neglected in the numerical model with solid TNT. With this simplification, the model can be built much smaller (0.4×0.4×2.0 m, "small model" in Figure 14) than the numerical model used e.g. by Coussin [41]. Absorbing elements replace the ignored air. All models use symmetry conditions; only one eighth of the geometry is built.

The solid TNT model is meshed with cube finite volumes with a second-order approach in both space and time. The centre of the explosive is built

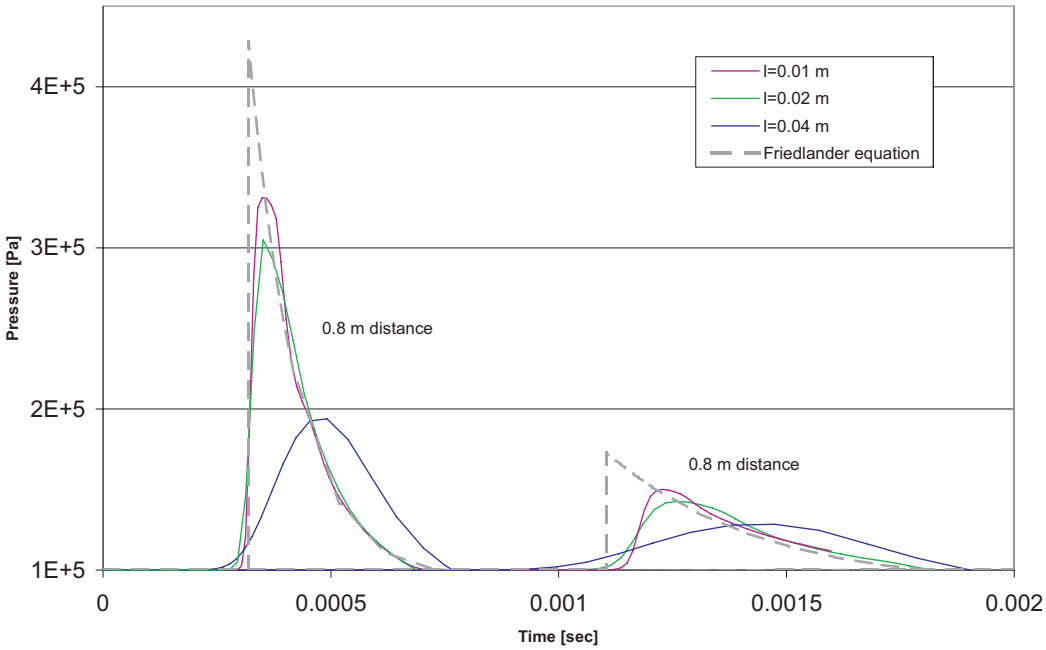

Figure 13: Influence of mesh size – pressure

as a cube with 7 (coarse mesh) or 10 (fine mesh) finite volumes along each direction. Around this cube, the mesh is generated in a similar way to the model in Section 3.5.1. This leads to a spherical charge. The space between the spherical charge and a bigger cubic box around the charge (see Figure 14) is also filled with cubic volumes and is defined as air using the ideal gas law. The explosive is modelled by the JWL equation and the parameters shown in Table 1.

For the calculations with the balloon method, two different balloon sizes are used: one with a volume of $1.0 \cdot 10^{-3}\,\mathrm{m}^3$ (corresponding pressure $9.44 \cdot 10^7$ Pa), and the other one with a volume of $2.8 \cdot 10^{-3}\,\mathrm{m}^3$ (corresponding pressure $2.74 \cdot 10^7$ Pa). Both models are built with larger dimensions ($1.2 \times 0.8 \times 2.0$ m, "full model"), thus taking also into account the reflection at the wall.

The experimental result obtained by Alia is shown in Figure 15, where it is compared with Kingery's pressure-time curve, which describes the peak pressure and the positive impulse very well. The pressure wave in the experiment is slower than the wave in Kingery's model. A reason could be that Kingery's experimental data is developed for TNT and not for C4. The experimental result of Alia shows also the reflection of the air blast wave at the wall, arriving at the gauge point 5.2 ms after the detonation of the charge.

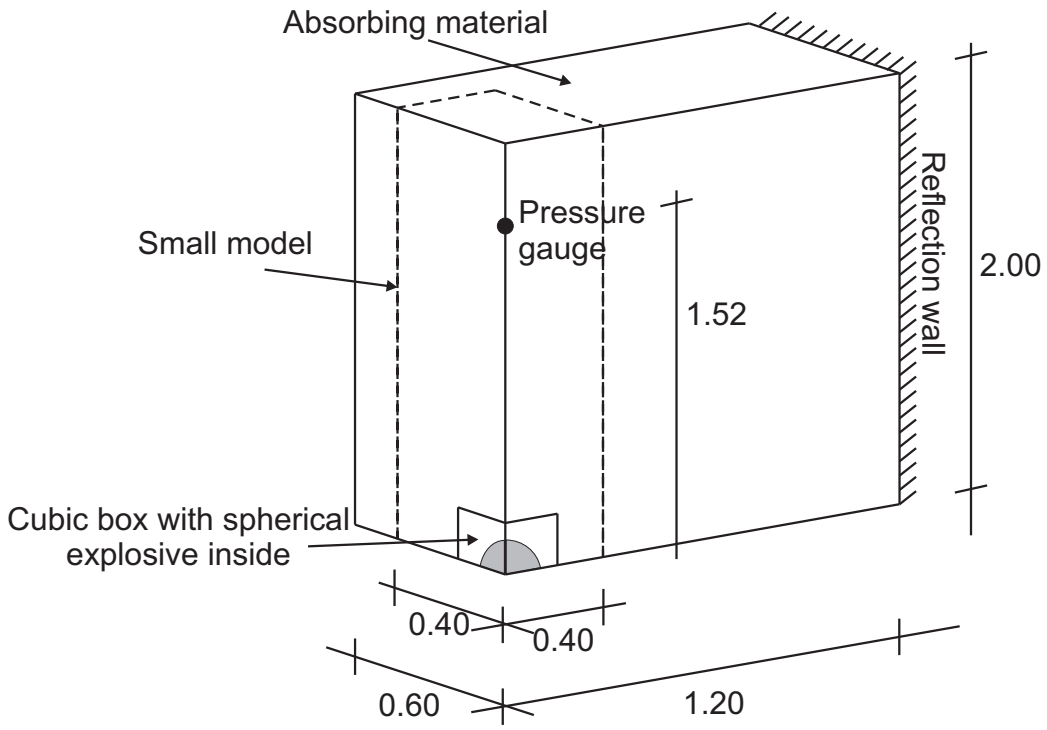

Figure 14: Model from Alia (dimensions in m)

The solid TNT model also shows a time shift which, however, is smaller than for Kingery's equation. The positive impulse is similar to the experimental one. However, the pressure drop in the negative phase is much faster than in Alia's experiment. The difference between the two meshes is observable but small, while the difference in the calculation time is dramatic (1.75 h to 19.6 h).

The impulse and the pressure-time curve of the compressed balloon method (full model) are similar to the experiment, if one disregards the time shift. The compressed balloon method with higher overpressure (smaller volume of the balloon) shows a larger time shift of the pressure wave than the model with the smaller overpressure. The pressure-time curve is shifted in Figure 16 to allow better comparison of the different parts of the curve. Comparison with the results of Coussin's finite volume calculations [41] shows that the compressed balloon method has the same behaviour but is much faster (about 1.3 h on a current desktop PC) in contrast with Coussin's finite volume solution (about 46 h on a similar processor, but with 8 times more memory).

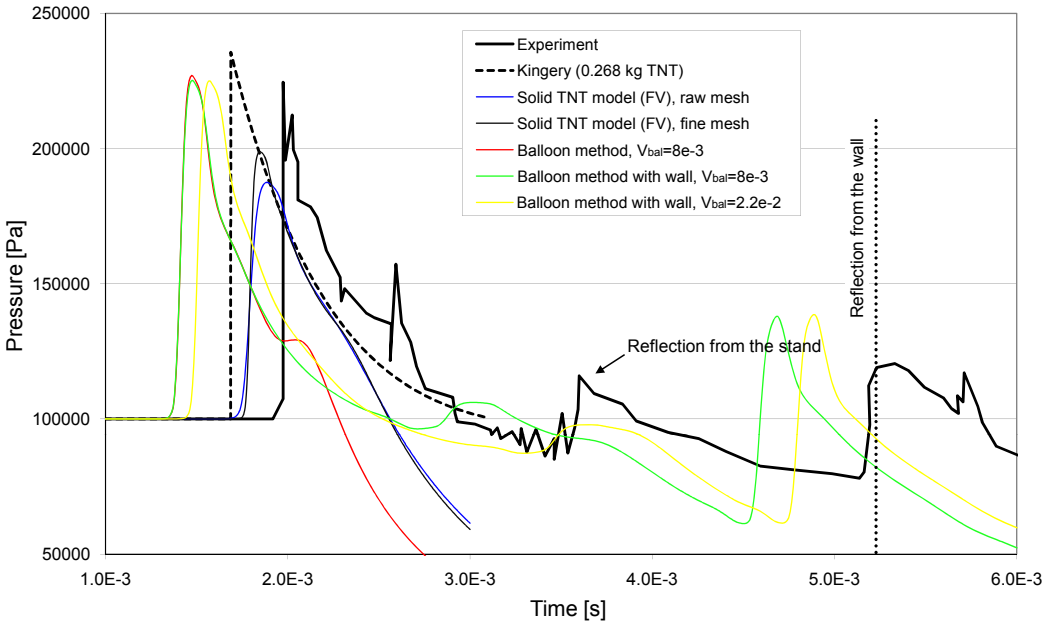

Figure 15: Results for the experimental model from Alia with different simulation methods

It can be seen, that the numerical solution follows in most parts Alia's experimental curve. If one neglects the time shift (which can also be seen in Kingery's equation), the compressed balloon method can represent the pressure-time curve very well. The reflection at the wall is fairly well represented, both in the arrival time and in the pressure magnitude.

It can be concluded that the compressed balloon method can be used to calculate this type of problems. The time shift in the numerical solutions could be partly due to the different kind of explosives. In any case, the shift has very little influence on the behaviour of the structure.

4.2 Urban Environment Experiment

Experiments with a detonation in an urban environment are used to verify the compressed balloon method in more complex geometries. Experimental tests with a scaled model (1:50) are carried out by Feng [42] and presented by Fairlie [15]. A charge with a size of 8 g TNT is located midway between two concrete blocks with dimensions of 2.0×0.15×0.16 m (see Figure 17). There are also two concrete blocks at the ends of this 'street' with a size of 0.3×0.3×0.3 m. The pressure-time functions are recorded at one point at

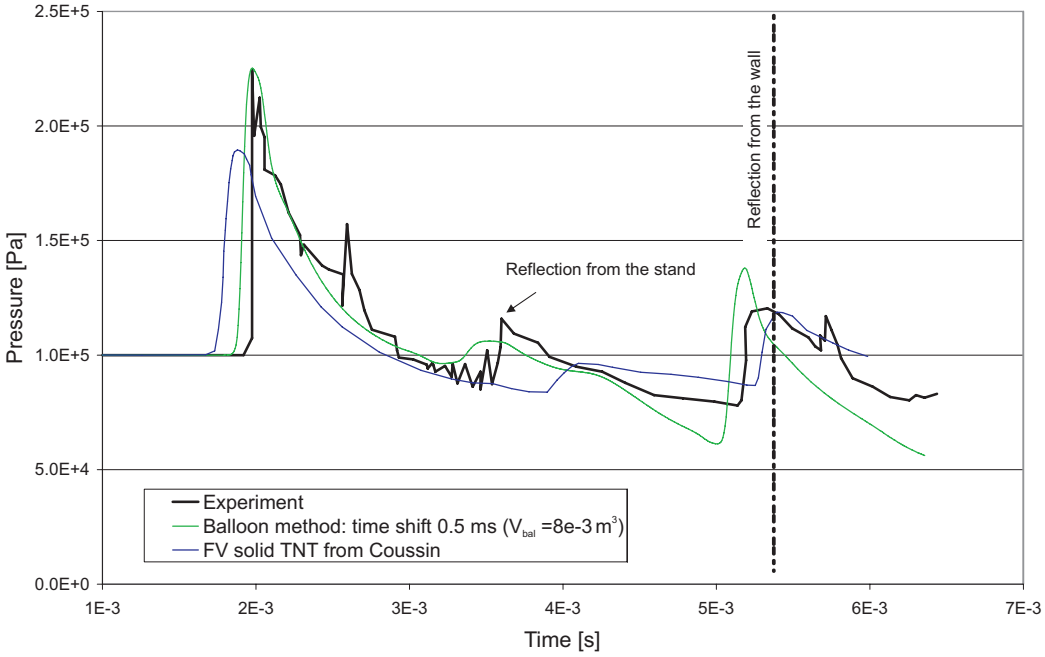

Figure 16: Results for the experimental model from Alia after shifting the numerical results of +0.5 ms

the end of the street and at another point around the corner of the building at the end of the street (see Figure 17).

One solid TNT model and two different compressed balloon models are used to calculate the development of the air blast wave in this geometry. All models use two symmetry conditions. The solid TNT model is built with tetrahedral finite volumes (second-order approach for the flux). The element size inside the explosive is chosen as 0.002 m, then it increases up to 0.02 m in the rest of the model. About 130,000 elements are used.

The first compressed balloon model is built with cube finite volumes with a constant element size of 0.01 m corresponding to about 126,000 elements. The other model uses about 179,000 tetrahedral finite volumes with a maximum size of 0.02 m. The balloon volume of both models is set to $9.6 \cdot 10^{-5}\,\mathrm{m}^3$, which corresponds to a pressure in the balloon of $5.44 \cdot 10^7$ Pa.

Figure 18 shows the development of the air blast wave by using the compressed balloon method (tetrahedral finite volumes). The air blast wave is reflected at 1.57 ms. The comparison between the numerical and the experimental results (Figure 19) at gauge location 1 shows that the pressure-time curve resulting from the solid TNT model underestimates the impulse as

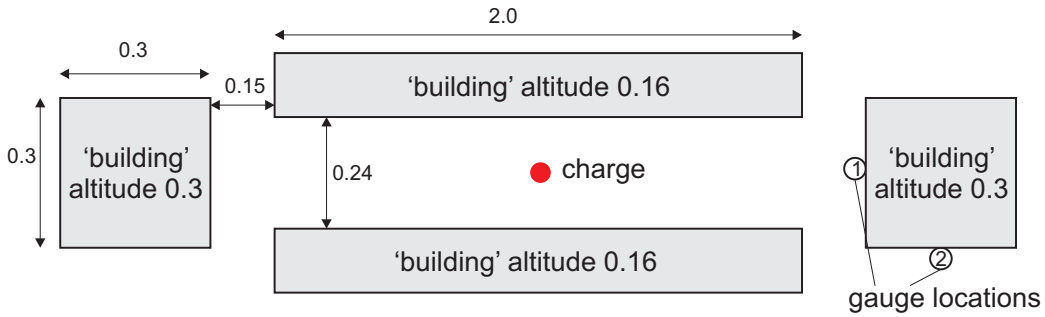

Figure 17: Urban Environment Model (dimensions in m)

well as the peak pressure. The finite volume model results in a fairly good pressure-time function. Both compressed balloon models show a good description of the pressure-time curve. The time shift of the tetrahedral finite volumes is bigger than when cube finite volumes are used.

The numerical results of the compressed balloon methods for the second gauge location (see Figure 20 show also a good correspondence with the experimental result, apart from the time shift. The pressure-time function of the finite volume solid TNT model underestimates the positive impulse. The pressure-time function proposed by Kingery cannot be used because Kingery neglects any street channelling effect and thus predicts much smaller pressures.

There is also a big difference in the calculation time. The solid TNT calculation needs approximately 7.2 h on a current desktop PC. Thanks to a much more regular mesh, the calculation time of the compressed balloon method is much smaller: 1.2 h with tetrahedral finite volumes and 0.6 h with cube finite volumes.

4.3 Calculations of a Metro Line Carriage

The compressed balloon method is also used to determine the influence of a detonation inside a metro line carriage.

In the past, most trains carriages were built with a substructure made from steel. Onto this substructure metal sheets are welded. Such design is very heavy and expensive to construct. The thickness of the metal sheets is in the order between 3 and 12 mm. Several current trains are built from extruded aluminium since weight can be reduced dramatically using this material and productivity can be increased.

The geometrical representation of the train carriage investigated is ob-

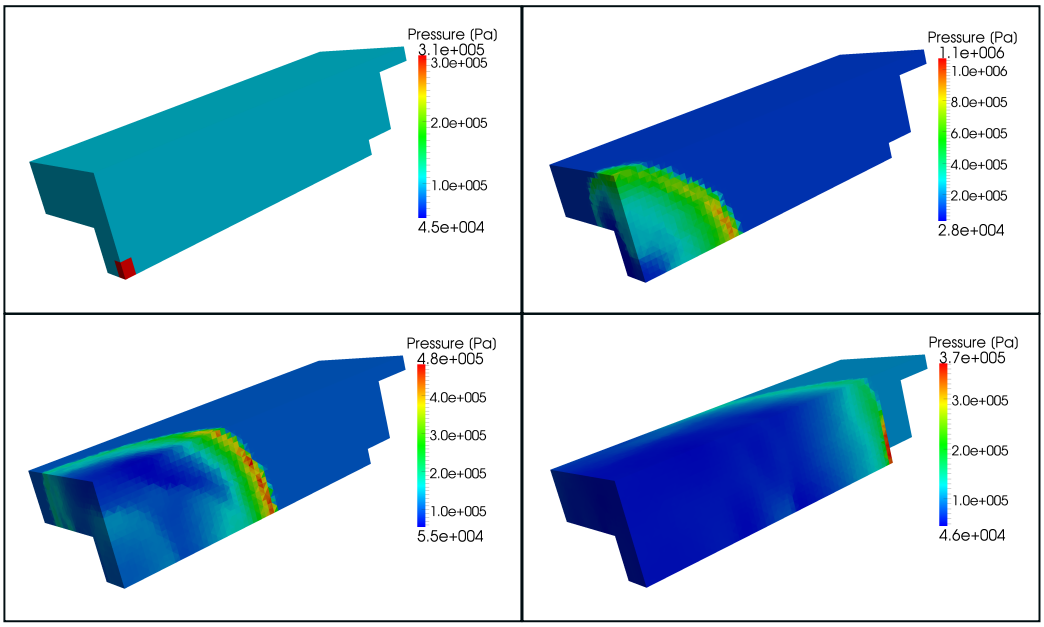

Figure 18: Urban Environment Model, compressed balloon method, t = 0.0; 0.24; 0.57; 1.59 ms

tained from on-site 3D laser scannings by the JRC 3D Reconstructor software (see Boström et al. [43]) and is shown in Figure 21. The length of the model is 14.7 m, the width of the train is 2.68 m, the height is 2.14 m.

An aluminum sheet of 3 mm thickness is welded on a frame structure. The aluminum sheet is modelled using quadrilateral shell elements. A Lagrangian formulation for all solid material is used. An erosion criterion is used for the aluminium sheets with a Van Mises failure limit of $245 \cdot 10^6$ Pa. The cross section of the frame structure tentatively has the standard profile IPE80. These profiles are placed near the doors and at the upper border of the carriage. The floor of all trains is considered rigid since it is a very stiff construction and since in most terrorist attacks the reported displacements and failure of the floor were small.

Laminated safety glass is used for the windows (for the simulation method see Larcher [44]). Since the failure of the laminated glass can not be represented with the element sizes used for the calculations, a displacement criterion of 30 % of the span of the windows is used. Reaching this limit, the border of the window is eroded so that the air can escape.

A charge of 10 kg TNT is located in the centre of the train. The diameter of the balloon is chosen to 0.7 m. The mesh size of the fluid mesh is set to

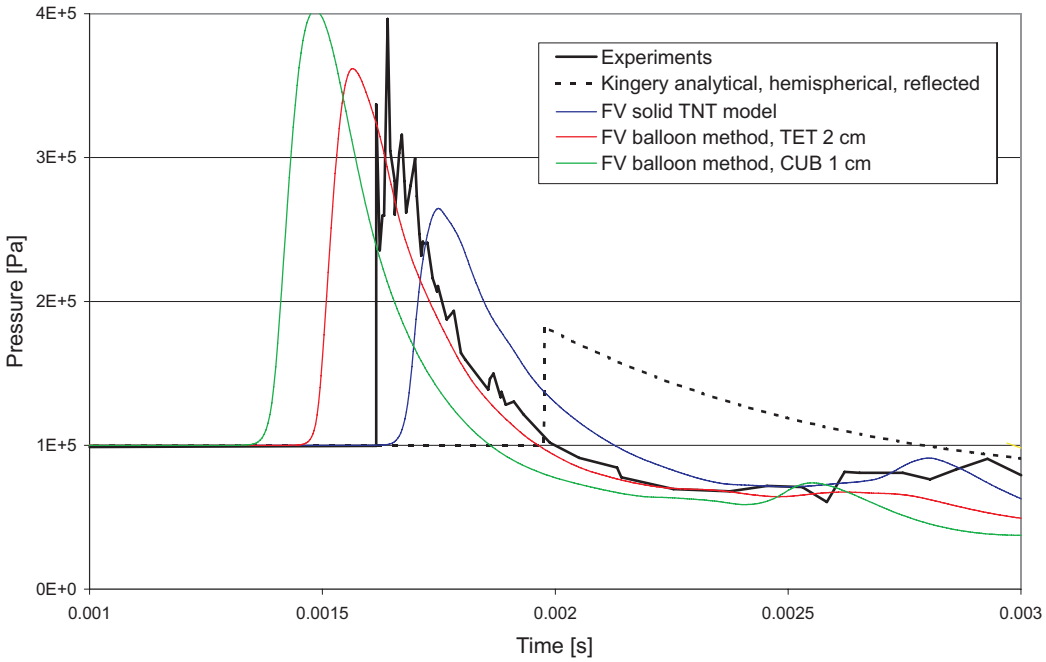

Figure 19: Urban Environment Model – results of several methods, gauge location 1

0.1 m, the mesh size of the structural part is set to a maximum of 0.1 m. Non-conforming fluid-structure interaction is used to allow calculation of the fluid even after failure and erosion of parts of the structure.

The development of the pressure, the displacements, and the failure of the structure are presented in Figure 22. The air blast wave resulting from the compressed balloon destroys the structure immediately around the explosive. At t = 13 ms all windows are failed due to reaching the failure criterion. The extremities of the carriage are also destroyed due to the channelling effect and the reflection of the wave at the closed ends. The reflection leads to higher peak pressures and impulses at the ends than in the other parts of the tube. In comparison to the terrorist attack in Madrid near Atocha station, where a charge of 8 to 12 kg was used, the failure of the structure is similar, even though the frame structure of the real train carriages involved is not known in detail. Using fluid-structure interaction the risk inside the train can also be calculated using the impulse and the pressure (see Larcher et al. [45]).

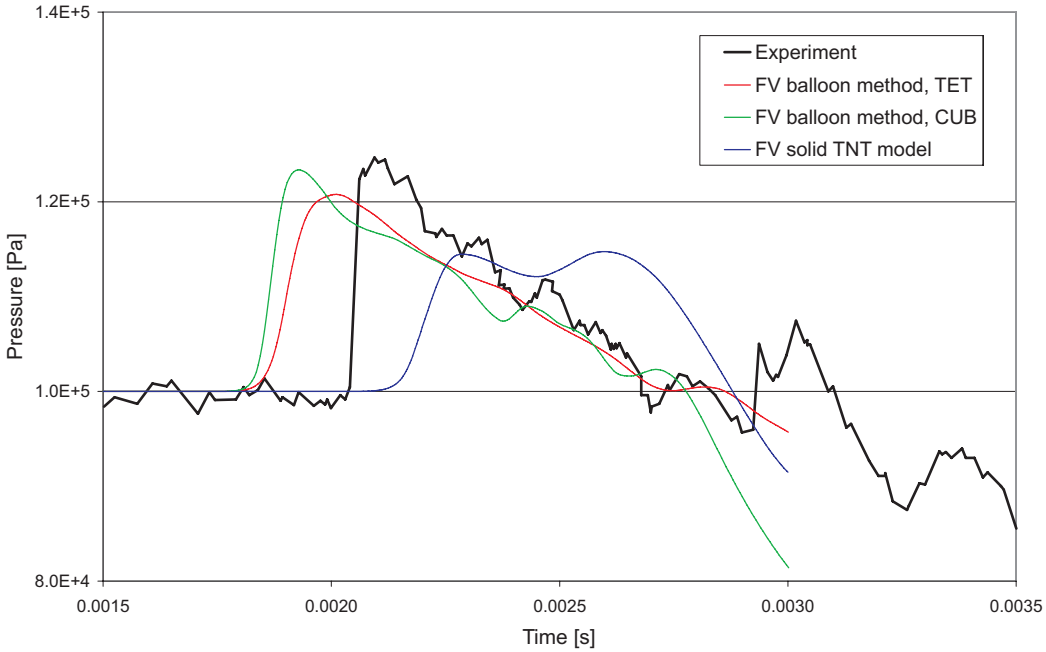

Figure 20: Urban Environment Model – results of several methods, gauge location 2

5 Conclusion

This paper presents several methods for simulating air blast waves, which can also be used inside complex structures. Developments are done to better fit the compressed balloon method to experimental data. This method allows a relatively fast calculation by taking into account reflections, shadowing and channelling. The overpressure of such a balloon can be calculated by simple equations presented in this paper. Several models with different balloon sizes, different element sizes and different geometries have shown that the compressed balloon method produces representative impulses and peak pressures. The limitation of the pressure ratio inside the balloon is discussed.

The compressed balloon method is only a phenomenological model. The method cannot therefore represent all kinds of possibilities. The pressure in the region nearby the balloon is not very accurate. The distance between the balloon and the structure should be large enough.

The implementation of the compressed balloon method in existing codes, which deal with fluid-structure interactions, is quite simple. The "real" explosive charge and part of the surrounding air inside a structure (balloon

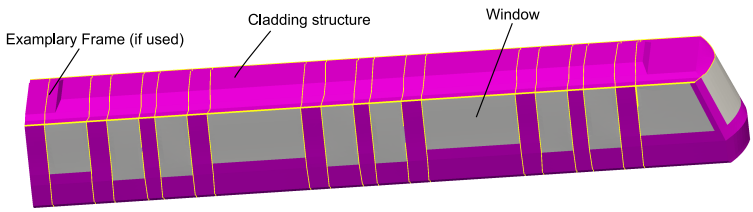

Figure 21: Structure of the single train carriage investigated

region) is replaced by air at a higher pressure. The remaining procedure is the same as using a solid TNT model. Experience has shown that the results of fluid calculations in several codes differ. The results of the compressed balloon method should therefore also be checked for other codes.

References

[1] E. L. Lee, H. C. Hornig, J. W. Kury, Adiabatic expansion of high explosive detonation products, Tech. Rep. No. UCRL-50422, Lawrence Radiation Laboratory (1968).

[2] B. Dobratz, P. Crawford, LLNL Explosives Handbook: Properties of Chemical Explosives and Explosive Simulants, Tech. Rep. UCRL-5299; Rev.2, University of California; Lawrence Livermore National Laboratory (1985).

[3] M. B. Liu, G. R. Liu, Z. Zong, K. Y. Lam, Computer simulation of high explosive explosion using smoothed particle hydrodynamics methodology, Computers and Fluids 32 (3) (2003) 305 – 322.

[4] D. A. Cendón, V. S. Gálvez, F. Gálvez, Modelling explosions using ALE meshes: The influence of mesh refinement in pressures and in efforts induced by blast/structure interaction, Structures and Materials 15 (2004) 173–180.

[5] A. Alia, M. Souli, High explosive simulation using multi-material formulations, Applied Thermal Engineering 26 (2006) 1032–1042.

[6] G. Langdon, G. Schleyer, Inelastic deformation and failure of profiled stainless steel blast wall panels. Part I: Experimental investigations, International Journal of Impact Engineering 31 (2005) 341–369.

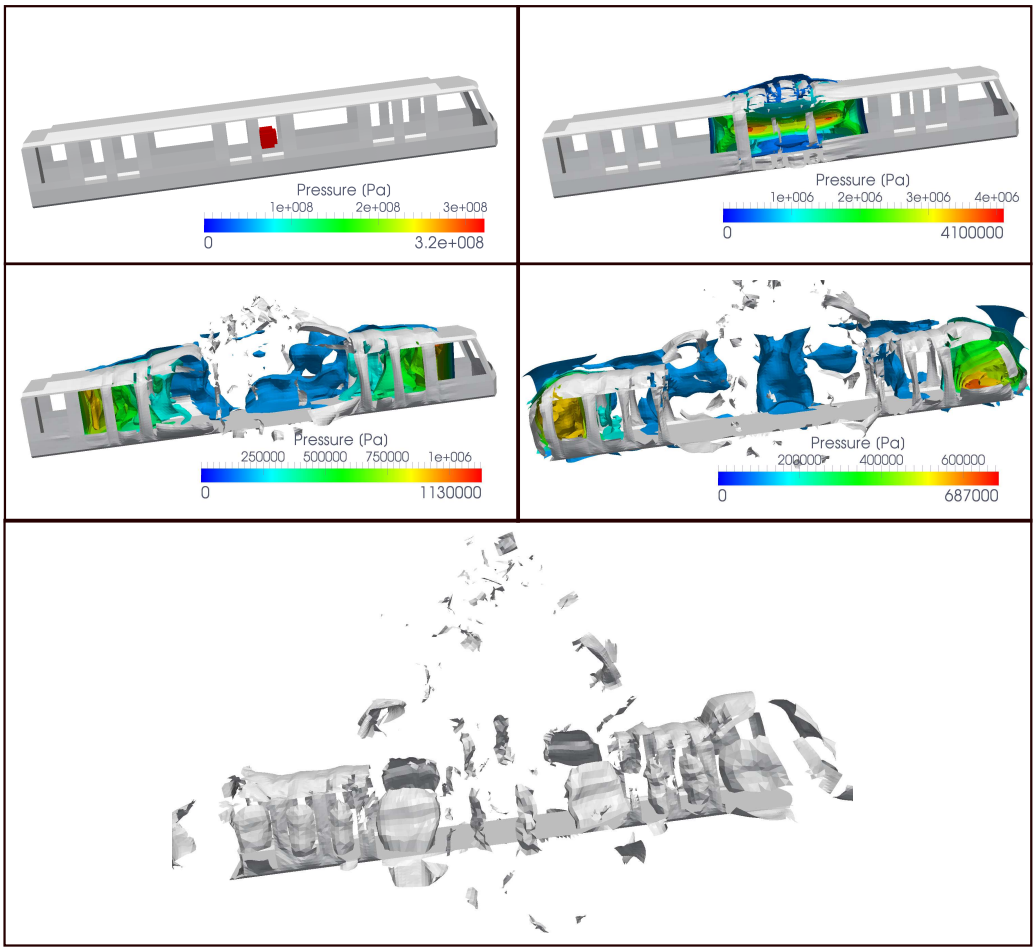

Figure 22: Metro Line Carriage – pressure at t = 0; 1; 4; 8 ms; displacements after 13 ms

[7] M. M. Gram, A. J. Clark, G. A. Hegemier, F. Seible, Laboratory simulation of blast loading on building and bridge structures, WIT Transactions on the Built Environment 87 (2006) 33–44.

[8] G. Langdon, G. Schleyer, Inelastic deformation and failure of profiled stainless steel blast wall panels. Part II: Analytical modelling considerations, International Journal of Impact Engineering 31 (2005) 371–399.

[9] B. M. Luccioni, R. D. Ambrosini, R. F. Danesi, Analysis of building collapse under blast loads, Engineering Structures 26 (1) (2004) 63 – 71.

[10] P. Smith, T. Rose, Blast loading and building robustness, Prog. Struct. Engng. Mater. 4 (2002) 213–223.

[11] X. Q. Zhou, H. Hao, Prediction of airblast loads on structures behind a protective barrier, International Journal of Impact Engineering 35 (5) (2008) 363–375.

[12] P. D. Smith, T. A. Rose, Blast wave propagation in city streets - an overview, Progress in Structural Engineering and Materials 8 (1) (2006) 16–28.

[13] A. M. Remennikov, T. A. Rose, Modelling blast loads on buildings in complex city geometries, Computers and Structures 83 (27) (2005) 2197–2205.

[14] P. D. Smith, G. C. Mays, T. A. Rose, K. G. Teo, B. J. Roberts, Small scale models of complex geometry for blast overpressure assessment, International Journal of Impact Engineering 12 (3) (1992) 345–360.

[15] G. E. Fairlie, Efficient analysis of high explosive air blast in complex urban geometries using the AUTODYN-2D and 3D hydrocodes, analytical and experimental methods, in: 15th Int. Symposium on the Military Aspects of Blast and Shock, 14-19 September, Banff, Canada, 1997.

[16] B. Luccioni, D. Ambrosini, R. Danesi, Blast load assessment using hydrocodes, Engineering Structures 28 (12) (2006) 1736–1744.

[17] W. Baker, Explosions in the Air, University of Texas Press, Austin and London, 1973.

[18] W. Baker, P. Cox, P. Westine, J. Kulesz, R. Strehlow, Explosion Hazards and Evaluation, Elsevier, Amsterdam, 1983.

[19] G. F. Kinney, K. J. Graham, Explosive Shocks in Air, Springer, Berlin; Heidelberg; New York; Tokyo, 1985.

[20] C. N. Kingery, G. Bulmash, Airblast parameters from TNT spherical air burst and hemispherical surface burst, Tech. rep., Defence Technical Information Center, Ballistic Research Laboratory, Aberdeen Proving Ground, Maryland (1984).

[21] D. Hyde, ConWep, US Army Waterways Experimental Station, US Army (1991).

[22] TM 5-855-1: Fundamentals of protective design for conventional weapons, Tech. rep., Waterways Experimental Station, US Army (1986).

[23] J. Drake, L. Twisdale, R. Frank, W. Dass, M. Rochefort, R. Walker, J. Britt, C. Murphy, T. Slawson, R. Sues, Protective construction design manual, Tech. Rep. ESL-TR-87-57, Air Force Engineering and Services Center, Tyndall Air Force Base, Florida (1989).

[24] Joint Research Centre (JRC), Commissariat à l'Énergie Atomique (CEA), http://europlexus.jrc.ec.europa.eu/, EUROPLEXUS User's manual (2009).

[25] P. Galon, Méthode des volumes finis pour les écoulements compressibles: Analyse bibliographique, Tech. Rep. RAPPORT DM2S, SEMT/DYN/RT/03-013/A, Commissariat à l'Énergie Atomique (CEA), Gif-sur-Yvette, France (2004).

[26] D. Benson, Computational methods in Lagrangian and Eulerian hydrocodes, Computer Methods in Applied Mechanics and Engineering 99 (1992) 235–394.

[27] F. Dubois, Discrétisation spatiale multidimensionnelle, Ph.D. thesis, Cours à l'Institut pour la Promotion des Sciences de l'Ingénieur (1992, édition révisée juillet 2003).

[28] D. Boris, J.P.; Book, Flux-corrected transport I. SHASTA, a fluid transport algorithm that works, Journal of Computational Physics 11 (1973) 38–69.

[29] Century Dynamics, AUTODYN Theory manual, 4th Edition (2005).

[30] F. Casadei, J. Halleux, Binary spatial partitioning of the central-difference time integration scheme for explicit fast transient dynamics, International Journal for Numerical Methods in Engineering 78 (12) (2009) 1436–1473.

[31] J. K. Clutter, M. Stahl, Hydrocode simulations of air and water shocks for facility vulnerability assessments, Journal of Hazardous Materials 106A (2004) 9–24.

[32] Century Dynamics, AUTODYN Remapping manual, 4th Edition (2005).

[33] N. K. Birnbaum, R. A. Clegg, G. E. Fairlie, C. J. Hayhurst, N. J. Francis, Analysis of blast loads on buildings, in: ASME pressure vessels

and piping conference: Structures under Extreme Loading Conditions, Montreal, Quebec, Canada, 1996.

[34] T. Rose, P. Smith, Influence of the principal geometrical parameters of straight city streets on positive and negative phase blast wave impulses, International Journal of Impact Engineering 27 (4) (2002) 359–376.

[35] T. Børvik, A. Hanssen, M. Langseth, L. Olovson, Response of structures to planar blast loads – a finite element engineering approach, Computers & Structures 87 (2009) 507–520.

[36] H. L. Brode, Numerical solutions of spherical blast waves, Journal of Applied Physics 26 (6) (1955) 766–775.

[37] D. Ritzel, K. Matthews, An adjustable explosion source model for CFD blast calculations, in: Proceedings to the 21st International Symposium on Shock Waves, Great Keppel Island, Australia, July 20-25, 1997, pp. 97–102.

[38] M. Omang, S. Borve, J. Trulsen, Alternative kernel functions for smoothed particle hydrodynamics in cylindrical symmetry, Shock Waves 14 (4) (2005) 293–298.

[39] S. Trelat, Impact de fortes explosions sur les bâtiment représentatifs d'une installation industrielle, Ph.D. thesis, Université d'Orleans (2006).

[40] G. Cusatis, D. Pelessone, A. Mencarelli, J. T. Baylot, Simulation of reinforced concrete structures under blast and penetration through lattice discrete particle modeling, in: ASME International Mechanical Engineering Congress and Exposition (IMECE) 2007, November 11-15, Seattle, USA, 2007.

[41] A. Coussin, P. Galon, Europlexus - volumes finis - introduction et validation de deux nouveaux matériaux pour modéliser les explosions, Tech. Rep. RAPPORT DM2S, SEMT/DYN/RT/08-002/A, Commissariat à l'Énergie Atomique (CEA), Gif-sur-Yvette, France (2008).

[42] L. Feng, Modelling blast in urban area, Tech. Rep. No. 11 MSc Weapons Effects on Structures Project Report, Cranfield University Weapons Effects on Structures, Royal Military College of Science, Shirivenham, UK, (1997).

[43] G. Boström, M. Fiocco, J. Gonçalves, D. Puig Alcoriza, V. Sequeira, B. Chartier, R. Kiesser, F. Mariotte, M. Richard, P. Zamora, 3D reconstruction in nuclear security, ESARDA Bulletin 38 (2008) 17–24.

[44] M. Larcher, Simulation of laminated glass loaded by air blast waves, in: DYMAT 2009 - 9th International Conferences on the Mechanical and Physical Behaviour of Materials under Dynamic Loading, EDP Sciences (www.dymat-proceedings.org), 2009, pp. 1553–1559.

[45] M. Larcher, F. Casadei, G. Solomos, Risk analysis of explosions in trains by fluid-structure calculations, Journal of Transportation Security, preprint, DOI: 10.1007/s12198-010-0038-z.

European Commission

EUR 24288 EN – Joint Research Centre – Institute for the Protection and Security of the Citizen
Title: Explosions in complex geometries - a comparison of several approaches
Authors: Martin Larcher, Folco Casadei
Luxembourg: Office for Official Publications of the European Union
2010 – 41 pp. – 21.0 x 29.7 cm
EUR – Scientific and Technical Research series – ISSN 1018-5593
ISBN 978-92-79-15245-0
DOI 10.2788/73796

Abstract
For the design and calculation of structures loaded by air blast waves, especially from inside the structure, assumptions on the applied load are needed. This paper presents several simulation methods for the air blast loading of structures and their ability to be used for complex geometries. Experimental-analytical pressure-time functions of spherical load conditions applied to the structure by disregarding the air are not applicable in such cases because they do not account for reflections, shadowing and channelling effects. Fluid calculations, which model also the solid explosive, are very expensive due to the extremely small elements for the explosive and the air nearby.

This paper therefore presents a review of a well-known simulation method, which uses a balloon with compressed air instead of the explosive. A procedure is developed which makes it possible to determine the overpressure of such a balloon for a given size of the explosive more accurately than before. The pressure-time function and the impulse-distance function of calculations using this method show good correspondence with experimental-analytical data. The functioning of the method is verified against experimental results.

How to obtain EU publications

Our priced publications are available from EU Bookshop (http://bookshop.europa.eu), where you can place an order with the sales agent of your choice.

The Publications Office has a worldwide network of sales agents. You can obtain their contact details by sending a fax to (352) 29 29-42758.

The mission of the JRC is to provide customer-driven scientific and technical support for the conception, development, implementation and monitoring of EU policies. As a service of the European Commission, the JRC functions as a reference centre of science and technology for the Union. Close to the policy-making process, it serves the common interest of the Member States, while being independent of special interests, whether private or national.

LB-NA-24288-EN-C